Condensate depletion in two-species Bose gases: A variational quantum Monte Carlo study

A. R. Sakhel,[1] J. L. DuBois,[2] and H. R. Glyde[3]

[1]*Faculty of Engineering Technology, Al-Balqa Applied University, Amman 11134, Jordan*
[2]*Department of Chemistry, University of California, Berkeley, 19 Gilman Hall, Berkeley, California 94720-1460, USA*
[3]*Department of Physics and Astronomy, University of Delaware, Newark, Delaware 19716, USA*

We investigate two-species Bose gases in traps with various interactions using variational quantum Monte Carlo (VMC) techniques at zero temperature. The bosons are represented by hard spheres whose diameter is equivalent to the *s*-wave scattering length in the low-energy and long-wavelength approximation. We explore the role of repulsive and attractive interspecies or intraspecies interactions on the condensate properties of the mixtures, particularly the condensate fraction of each species as compared to the case when each species is in a separate trap of its own. We model the repulsive interactions by a hard-core (HC) potential and the attractive interactions by a shallow model potential. The VMC density profiles and energies are evaluated at various interactions and two mass ratios of the species.

PACS number(s): 03.75.Mn, 05.30.Jp, 02.70.Ss, 64.75.−g

I. INTRODUCTION

The interest in the investigation of two-species Bose-Einstein condensates (2BECs) in traps has grown substantially since their first experimental realization in 1997 [1]. Since then, the literature on 2BECs in traps has exploded [2–20] and the interests are now drifting more strongly towards these mixtures [21,22], which are the major theme of this paper.

In this paper we investigate the role of interspecies and intraspecies interactions on the properties of two-species Bose gases (2BEC) in a tight isotropic harmonic trap at zero temperature using variational quantum Monte Carlo (VMC) methods. A tight trap enables us to simultaneously use a low number of particles and achieve high densities since the volume of the trapped cloud is much smaller than the usual size [23–25], where $a_{ho} \sim 10^4$ Å. Here $a_{ho} = \sqrt{\hbar/m\omega_{ho}}$ is the trap length where m is the mass of the boson, ω is the trapping frequency, and $\hbar$ is Planck's constant. We represent the bosons by hard spheres (HS) whose hard-core (HC) diameter is equivalent to the *s*-wave scattering length in the low-energy and long-wavelength approximation. In order to describe the interactions, we use a HS potential for repulsive, and a shallow two-body model potential for attractive interactions. Based on this, we emphasize the qualitative nature of the present work and deemphasize comparisons with current experiments. The results stand alone as qualitative properties of the model system. A key point in our present research is that we do not use the scattering length in describing attractive interactions as is usually done in mean-field investigations, but rather the depth of a two-body model potential as justified later on. We thus vary the depth of the model potential and HC diameters of the bosons and investigate the resulting properties such as the VMC energies and density distributions. We particularly focus on the VMC condensate fractions and condensate density profiles in an—and to the best of our knowledge—unprecedented manner in the literature concerning mixtures of Bose gases. Another key point here is that we focus on the factors that enhance the condensate depletion of the 2BEC components. We find

chiefly that the mixing of two Bose gases in a trap enhances the depletion of the condensates of each gas as compared to the case when either one is in a separate trap of its own. Thus the one-component Bose gas (1BEC) in our paper works chiefly as a *reference system* to which we compare our mixtures. Further, we find that no phase separation can occur in the case of attractive interspecies interactions and that two Bose gases cannot be mixed in the case of large repulsive interspecies interactions. Some of our findings are similar to those of Kim and Lee [26] and Shchesnovich *et al.* [4]. Our work is particularly related to the work of Ma and Pang [17] who did an investigation similar to ours except that they used repulsive interactions only, whereas we additionally use attractive interactions. We further evaluate the energies of the systems and check them against an approximate model calculation.

On the theoretical side, there have been many theories and investigations. For example, Kim and Lee [26] examined the stability properties of the ground state of 2BECs as a function of interspecies interactions. One of the ground states that they found had a component localized at the center of the trap surrounded by the other component thereby forming a core and shell. Ho and Shenoy [6] discussed binary mixtures of alkali condensates and found that the heavier of the two components always enters into the interior of the trap and the lighter component is usually pushed towards the edges of the trap. Chui *et al.* [9] investigated the nonequilibrium spacial phase segregation process of a mixture of alkali BECs. Pu and Bigelow [7] presented theoretical studies of a 2BEC. They showed that a mixed Bose gas displays novel behavior not found in a pure condensate and that the structure of the density profiles is very much influenced by the interactions.

On the experimental side, there also have been many investigations. For example, Modugno *et al.* [27] reported the realization of a mixture of BECs of two different atomic species using potassium and rubidium by means of sympathetic cooling. Again Modugno *et al.* [28] reported on the Bose-Einstein condensation of potassium atoms achieved by sympathetically cooling the potassium gas with evaporatively cooled rubidium. Mudrich *et al.* [29] explored the thermodynamics in a mixture of two different ultracold Bose

043627-1

gases. They showed that a hot gas can be cooled to a lower temperature by mixing it with another colder gas. Maddaloni *et al.* [30] demonstrated an experimental method for a sensitive and precise investigation of the interaction between two condensates. They studied the effects of interaction by studying two completely overlapping condensates and found that the center-of-mass oscillations of the two condensates are damped if they are interacting and otherwise, if they are noninteracting. Matthews *et al.* [31] presented the experimental realization and imaging of a vortex in a two-component BEC. They induced the vortices by a transition between two spin states by hyperfine splitting of ^{87}Rb using a two-photon microwave pulse. Again, Matthews *et al.* [32] explored the dynamical response of a BEC due to a sudden change in the interaction strength and presented a method for the creation of condensate mixtures using radio frequency and microwave fields. Further, they observed an oscillatory behavior of the condensate sizes when the interactions are changed.

Although the above revealed some of the most important properties of ultracold mixed atomic systems in traps, an investigation of the condensate properties and energies is still missing. For example, what is the role of the hard core (HC) of the atoms in one component in determining the condensate fraction of the other component? In previous publications [33,34], it has been shown that the hard core (HC) of the bosons plays a fundamental role in depleting the condensate of a one-species Bose gas in a trap. Another issue which has not been addressed before is the role of the mass ratio of the bosons in a mixture in determining the condensate fractions and we briefly address this issue in this paper.

The paper is organized as follows. In Sec. II we present the method we used. In Sec. III we outline our results and in Sec. IV we discuss them and connect to the previous literature. In Sec. V we list our conclusions and in Appendix A we present a model for the estimation of the energies.

II. METHOD

We consider ultracold two-species Bose gases (2BEC) of N_1 and N_2 particles, masses m_1 and m_2, and HC diameters a_c and b_c, respectively, confined in a spherically symmetric tight harmonic trap. The total number of particles $N = N_1$
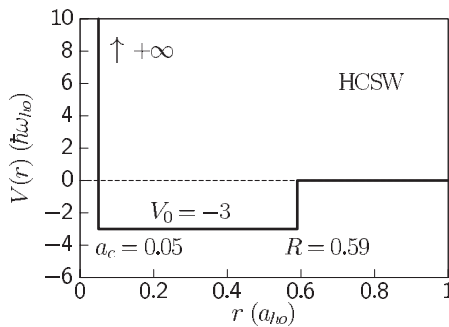

FIG. 1. HCSW interatomic potential with $a_c = 0.05$, attractive well range $R - a_c = 0.54$, and a potential depth $V_0 = -3$. For $r \leq a_c$, $V(r)$ is infinite. All lengths and energies are in trap units, $a_{ho} = \sqrt{\hbar/m\omega_{ho}}$ and $\hbar\omega_{ho}$, respectively.

$+ N_2$ is kept fixed and we use small numbers of particles since larger ones increase the computational times substantially. We investigate the 2BECs using variational quantum Monte Carlo (VMC) methods at zero temperature. The program for VMC used in earlier publications [33,34] and for the one-body density matrix (OBDM) [33] has been modified to accommodate 2BECs. We shall not explain the VMC technique as it can be found in a large number of references, rather we present our trial wave function and mention briefly how the particles are moved and how the densities are calculated.

A. Hamiltonian

The Hamiltonian of a two-component Bose gas is

$$H = \sum_{i=1}^{N_1} \left(-\frac{\hbar^2}{2m_1}\nabla^2_{r_{1i}} + \frac{1}{2}m_1\omega_1^2 r_{1i}^2 \right)$$
$$+ \sum_{j=1}^{N_2} \left(-\frac{\hbar^2}{2m_2}\nabla^2_{r_{2j}} + \frac{1}{2}m_2\omega_2^2 r_{2j}^2 \right) + \sum_{i<j} V_{11}^{int}(|\mathbf{r}_{1i} - \mathbf{r}_{1j}|)$$
$$+ \sum_{k<\ell} V_{22}^{int}(|\mathbf{r}_{2k} - \mathbf{r}_{2\ell}|) + \sum_{m,n} V_{12}^{int}(|\mathbf{r}_{1m} - \mathbf{r}_{2n}|), \quad (1)$$

where m_1 and m_2 are the individual masses of the atoms, $\mathbf{r}_{\sigma 1}, \ldots, \mathbf{r}_{\sigma N_\sigma}$ are the particle position-vectors from the center of the trap of components $\sigma = 1$ and 2, ω_1 and ω_2 are the trapping frequencies, V_{11}^{int} and V_{22}^{int} are the intraspecies interactions of species 1 and 2, respectively, and V_{12}^{int} is the interspecies interaction.

B. Units

We take length and energy in units of the trap $a_{ho} = \sqrt{\hbar/m\omega_{ho}}$ and $\hbar\omega_{ho}$, respectively, where $m = m_1$ and $\omega_{ho} = \omega_1$ are the mass and trapping frequency of component 1, respectively. Using these units $[H \rightarrow H/(\hbar\omega_{ho}) = \widetilde{H}, \ r \rightarrow r/a_{ho} = \widetilde{r}]$, the Hamiltonian (1) can be rewritten in the form

$$\widetilde{H} = \frac{1}{2}\sum_{i=1}^{N_1} (-\widetilde{\nabla}^2_{r_{1i}} + \widetilde{r}_{1i}^2) + \frac{1}{2}\sum_{j=1}^{N_2} \left[-\frac{m_1}{m_2}\widetilde{\nabla}^2_{r_{2j}} + \frac{m_2}{m_1}\left(\frac{\omega_2}{\omega_1}\right)^2 \widetilde{r}_{2j}^2 \right]$$
$$+ \sum_{i<j} \widetilde{V}_{11}^{int}(|\widetilde{\mathbf{r}}_{1i} - \widetilde{\mathbf{r}}_{1j}|) + \sum_{k<\ell} \widetilde{V}_{22}^{int}(|\widetilde{\mathbf{r}}_{2k} - \widetilde{\mathbf{r}}_{2\ell}|)$$
$$+ \sum_{m,n} \widetilde{V}_{12}^{int}(|\widetilde{\mathbf{r}}_{1m} - \widetilde{\mathbf{r}}_{2n}|), \quad (2)$$

thus introducing two ratios (m_1/m_2) and $(m_2\omega_2^2/m_1\omega_1^2)$ into the Hamiltonian.

C. HCSW interactions

We model the two-body interactions by using a hard-core square well (HCSW) potential. Essentially, it is a hard core plus an attractive tail added to it. Figure 1 shows our model potential where $V(r)$ is the depth and r is the two-body interparticle distance, all in units of the trap. Here, for example, the bosonic HC diameter is $a_c = 0.05$, the depth is $V_0 = -3$, and the range is $d = R - a_c$, which we keep fixed at

0.54. This range is of the same order of magnitude as that used in a previous work [35] for another potential and we return to this point in Sec. IV D. In this paper we are chiefly interested in using the depth of the HCSW to describe the interactions and not the associated scattering length. Nevertheless, we check the stability of the systems at the first Feshbach resonance when $a \rightarrow \pm \infty$ in Sec. IV E later on.

D. Trial wave function

The general form of the trial wave function is

$$\Psi_T(\{\mathbf{r}_1\},\{\xi_{11}\};\{\mathbf{r}_2\},\{\xi_{22}\};\{\xi_{12}\}) = \prod_{m=1}^{N_1} \prod_{n=1}^{N_2} f_{12}(|\mathbf{r}_{1m} - \mathbf{r}_{2n}|) \prod_{\sigma} [\prod_{i=1}^{N_\sigma} g_\sigma(\mathbf{r}_{\sigma i}) \prod_{i<j}^{N_\sigma} f_{\sigma\sigma}(|\mathbf{r}_{\sigma i} - \mathbf{r}_{\sigma j}|)], \qquad (3)$$

where $\{\mathbf{r}_\sigma\} \equiv (\mathbf{r}_{\sigma 1}, \ldots, \mathbf{r}_{\sigma N_\sigma})$, $g_\sigma(\mathbf{r}_{\sigma i})$ are single-particle wave functions for particles of type $\sigma = 1, 2$, and $f_{\sigma_1 \sigma_2}$ are pair correlation functions for intraspecies and interspecies interactions with variational parameters given by the sets $\{\xi_{\sigma_1 \sigma_2}\} = \{\beta_{\sigma_1 \sigma_2}, \gamma_{\sigma_1 \sigma_2}, \epsilon_{\sigma_1 \sigma_2}\}$. Here the pairs $\{\sigma_1, \sigma_2\}$ are $\{11\}$ and $\{22\}$ for intraspecies, and $\{12\}$ or $\{21\}$ for interspecies interactions. There can be several choices for the Jastrow functions depending on the interatomic interactions. In our case we constructed a flexible Jastrow function inferred from the exact solution of two particles interacting via a HCSW potential,

$$f_{\sigma_1 \sigma_2}(r_{ij}) = \begin{cases} 0, & r_{ij} \leq a_{\sigma_1 \sigma_2} \\ \dfrac{A_{\sigma_1 \sigma_2} \sin[\gamma_{\sigma_1 \sigma_2}(r_{ij} - a_{\sigma_1 \sigma_2})]}{r_{ij}}, & a_{\sigma_1 \sigma_2} < r_{ij} \leq r_{\sigma_1 \sigma_2 0} \\ 1 + \beta_{\sigma_1 \sigma_2}^2 \exp[-\epsilon_{\sigma_1 \sigma_2}(r_{ij} - r_{\sigma_1 \sigma_2 0})^2], & r_{ij} > r_{\sigma_1 \sigma_2 0}, \end{cases} \qquad (4)$$

where $r_{\sigma_1 \sigma_2 0}$ is the position of the maximum of the Jastrow function and $a_{\sigma_1 \sigma_2}$ is the HC diameter, where $a_{11} = a_c$, $a_{22} = b_c$, and $a_{12} = a_{21} = (a_c + b_c)/2$. The sinusoidal part of Eq. (4) is taken similar to the exact solution of two particles colliding inside a HCSW with relative energy $E_{\sigma_1 \sigma_2} = \hbar^2 k_{\sigma_1 \sigma_2}^2/(2\mu_{\sigma_1 \sigma_2})$ and HC diameter $a_{\sigma_1 \sigma_2}$ by replacing the HCSW wave vector $K_{\sigma_1 \sigma_2} = \sqrt{2\mu_{\sigma_1 \sigma_2}(V_{\sigma_1 \sigma_2} + E_{\sigma_1 \sigma_2})/\hbar^2}$ for each type of interaction of strength $V_{\sigma_1 \sigma_2}$ by a variational parameter $\gamma_{\sigma_1 \sigma_2}$. This is in order to decouple the Jastrow functions from their HCSWs and to introduce some flexibility to them. Another reason for this replacement is that we do not know the values of $E_{\sigma_1 \sigma_2}$ at the higher densities and we therefore allow $\gamma_{\sigma_1 \sigma_2}$ to vary slightly in order to indirectly imply a value for $E_{\sigma_1 \sigma_2}$. {Here $\mu_{11} = m_1$, $\mu_{22} = m_2$, and $\mu_{12} = m_1 m_2/(m_1 + m_2)$.} In our simulations, the optimized $\gamma_{\sigma_1 \sigma_2}$ is always very close to $K_{\sigma_1 \sigma_2}$ and $\gamma_{\sigma_1 \sigma_2} \geq K_{\sigma_1 \sigma_2}$. Thus attractive interaction between the particles is included in the Jastrow via $\gamma_{\sigma_1 \sigma_2}$. We then join the sinusoidal part at $r_{ij} = r_{\sigma_1 \sigma_2 0}$ to another function which decays to 1 in the long range. Note then that $r_{\sigma_1 \sigma_2 0}$ is not necessarily equal to $R_{\sigma_1 \sigma_2}$, the edge of the HCSW for each interaction type, and depending on the well depth it can be either inside or outside the HCSW. The reason for this construction is to provide smooth Jastrow functions whose maxima are at interparticle distances large enough to bring the bosons close together. Further, it is important to note that the attraction between the bosons is mainly caused by the Jastrow function (4), particularly by the "bump" of the Jastrow, which is higher than 1 at $r = r_{\sigma_1 \sigma_2 0}$. The part of the Jastrow function in the range $a_{\sigma_1 \sigma_2} < r_{ij} \leq r_{\sigma_1 \sigma_2 0}$ is then repulsive, whereas in the range $r_{ij} \geq r_{\sigma_1 \sigma_2 0}$ it is attractive. Note that in the case of only repul-

sive interactions the HCSW depths $V_{\sigma_1 \sigma_2}$ and $\beta_{\sigma_1 \sigma_2}$ are set to zero. Therefore, when $\gamma_{\sigma_1 \sigma_2} \rightarrow 0$,

$$\lim_{\gamma_{\sigma_1 \sigma_2} \rightarrow 0} \frac{\sin[\gamma_{\sigma_1 \sigma_2}(r_{ij} - a_{\sigma_1 \sigma_2})]}{\gamma_{\sigma_1 \sigma_2} r_{ij}} = \left(1 - \frac{a_{\sigma_1 \sigma_2}}{r_{ij}}\right) \qquad (5)$$

brings us back to the HS Jastrow function. $A_{\sigma_1 \sigma_2}$ (and $r_{\sigma_1 \sigma_2 0}$) are parameters that join the Jastrow in the interparticle-separation range $a_{\sigma_1 \sigma_2} < r_{ij} \leq r_{\sigma_1 \sigma_2 0}$ to that in the range $r_{ij} > r_{\sigma_1 \sigma_2 0}$ for the same slope and amplitude. For the single-particle wave functions, we use Gaussians of the form

$$g_\sigma(\mathbf{r}_{\sigma i}) = \exp(-\alpha_\sigma r_{\sigma i}^2), \qquad (6)$$

where α_σ are variational parameters. Later on in this paper we shall see that even with Gaussians centered at the origin, the variational wave function (3) is still able to describe phase separation. This indicates that the trial wave function is dominated by the pair correlation functions $f_{\sigma_1 \sigma_2}$ rather than the single-particle functions. In fact the Gaussians chiefly cause the density to vanish at the edges of the cloud thus indirectly confining the cloud within a certain volume.

E. Moving the particles

The particles are moved according to

$$\mathbf{r}'_{\sigma i} = \mathbf{r}_{\sigma i} + \Delta \mathbf{r}_\sigma(\eta - 0.5), \qquad (7)$$

where $\mathbf{r}'_{\sigma i}$ are new positions, η is a random number between 0 and 1, and $\Delta \mathbf{r}_\sigma$ are step size vectors which are adjusted to obtain optimal diffusion through configuration space—i.e., to obtain a VMC acceptance rate of $\approx 50\%$. After each update

of the particle coordinates the proposed move is either accepted or rejected according to the Metropolis, Rosenbluth, Rosenbluth, Teller, and Teller $[\mathrm{M(RT)}^2]$ [36] algorithm where the square of the trial wave function is used as the probability distribution from which particle configurations are sampled.

F. Minimization of the variance of the energy

In order to optimize the trial wave function, we numerically minimize the variance of the energy σ_E with respect to the variational parameters of the trial wave function. The variance is given by $\sigma_E^2 = \langle E^2 \rangle - \langle E \rangle^2$, where in general, for any operator O,

$$\langle O \rangle = \frac{\int d\mathbf{r}_1 d\mathbf{r}_2 |\Psi_0|^2 \left(\frac{O\Psi_1}{\Psi_1} \right) \frac{|\Psi_1|^2}{|\Psi_0|^2}}{\int d\mathbf{r}_1 d\mathbf{r}_2 |\Psi_0|^2 \frac{|\Psi_1|^2}{|\Psi_0|^2}}, \quad (8)$$

with $\Psi_0 = \Psi(\{\mathbf{r}_1\}, \{\xi_{11}^0\}; \{\mathbf{r}_2\}, \{\xi_{22}^0\}; \{\xi_{12}^0\})$ and $\Psi_1 = \Psi(\{\mathbf{r}_1\}, \{\xi_{11}\}; \{\mathbf{r}_2\}, \{\xi_{22}\}; \{\xi_{12}\})$ and $\int d\mathbf{r}_1 \equiv \Pi_{i=1}^{N_1} \int d^3 r_{1i}$, $\int d\mathbf{r}_2 \equiv \Pi_{j=1}^{N_2} \int d^3 r_{2j}$. Here $|\Psi_1|^2 / |\Psi_0|^2$ are weights used for the reweighting process of the variable O. $\{\xi_{\sigma_1 \sigma_2}^0\}$ are the initial and $\{\xi_{\sigma_1 \sigma_2}\}$ the optimized sets of variational parameters. In the Gaussians we also use the initial α_σ^0 and the optimized α_σ.

G. Condensate fraction

In the systems considered here we have two condensate fractions $n_0^{(1)}$ and $n_0^{(2)}$ for components 1 and 2, respectively. The overall condensate fraction of the mixture is $(n_0^{(1)} N_1 + n_0^{(2)} N_2)/(N_1 + N_2)$ but we only focus on the individual $n_0^{(1)}$ and $n_0^{(2)}$. The condensate fraction of each component is evaluated by calculating the eigenvalues of the natural orbitals using the one-body density matrix (OBDM) of each component in a manner similar to a calculation by DuBois and Glyde [33]. By using the trial wave function of Sec. II D, we evaluate the OBDM for components 1 and 2, respectively, as follows. In order to make the equations more compact, we define

$$Q_1(r_{11}, \ldots) = \psi(r_{11}, r_{12}, \ldots, r_{1N_1}, \{\xi_{11}\}; \{\mathbf{r}_2\}, \{\xi_{22}\}; \{\xi_{12}\}),$$

$$Q_1(r_{11}', \ldots) = \psi(r_{11}', r_{12}, \ldots, r_{1N_1}, \{\xi_{11}\}; \{\mathbf{r}_2\}, \{\xi_{22}\}; \{\xi_{12}\}),$$

$$Q_2(r_{21}, \ldots) = \psi(\{\mathbf{r}_1\}, \{\xi_{11}\}; r_{21}, r_{22}, \ldots, r_{2N_2}, \{\xi_{22}\}; \{\xi_{12}\}),$$

$$Q_2(r_{21}', \ldots) = \psi(\{\mathbf{r}_1\}, \{\xi_{11}\}; r_{21}', r_{22}, \ldots, r_{2N_2}, \{\xi_{22}\}; \{\xi_{12}\}).$$

Hence the OBDMs are written

$$\rho_a(r_{11}, r_{11}') = \frac{\prod_{i=2}^{N_1} \int d^3 r_{1i} \prod_{j=1}^{N_2} \int d^3 r_{2j} Q_1(r_{11}, \ldots) Q_1(r_{11}', \ldots)}{\langle \psi | \psi \rangle}, \quad (9)$$

leaving out the integration over r_{11} and r_{11}' and

$$\rho_b(r_{21}, r_{21}') = \frac{\prod_{i=1}^{N_1} \int d^3 r_{1i} \prod_{j=2}^{N_2} \int d^3 r_{2j} Q_2(r_{21}, \ldots) Q_2(r_{21}', \ldots)}{\langle \psi | \psi \rangle}, \quad (10)$$

leaving out r_{21} and r_{21}'. Here

$$\langle \psi | \psi \rangle = \int dr_1 \int dr_2 |\psi(\{\mathbf{r}_1\}, \{\xi_1\}; \{\mathbf{r}_2\}, \{\xi_2\}; \{\xi_{12}\})|^2$$

is the normalization factor and $\xi_{\sigma_1 \sigma_2}$ are the optimized variational parameters. Hence we extract the OBDM for each component from the two-body density matrix (TBDM) of the mixture by integrating out the contribution from the other component. In a manner similar to Ma and Pang [17] then, each component is essentially treated as a subspecies with its own properties but still it is not independent of the other species as a result of the interspecies interactions. The interspecies interactions are included in the OBDM through the interspecies Jastrow function f_{12}. From the trial wave function we can verify that Eqs. (9) and (10) reduce to the one-component case if the interspecies interactions are turned off. That is, the interspecies Jastrow function f_{12} becomes equal to 1 and the two components become independent of each other as they are now noninteracting.

H. Density profiles

The densities are calculated during a VMC run by dividing the space along the radial direction into spherical shells (bins) concentrated at the center of the trap and collecting the particles of each species in them as was done before by DuBois and Glyde [33].

III. RESULTS

In what follows we present the results of our Monte Carlo simulations. We display and discuss the resulting VMC density profiles and the condensate fractions of our mixtures with various interactions. We further compare the condensate fractions of the mixtures with the condensate fractions of their components when either one is in *a separate trap of its own*. We compare our VMC energies with the results from an approximate mean-field model derived in Appendix A. We further reveal the role of the mass ratio m_1/m_2 in determining some properties of the Bose gases. The trapping frequency is set to be the same for both components ($\omega_1 = \omega_2$) and the mass ratio is arbitrarily chosen to be $m_1/m_2 = 1.200$.

A. Stability of the mixtures as compared to one-species Bose gases

During the numerical optimization of the variational parameters as explained in Sec. II F, we plot the energy E_{VMC}/N versus the set of variational parameters $\{\xi_{\sigma_1 \sigma_2}\}$ used in our wave function. The numerical optimization process changes the variational parameters over several iterations and searches for a minimum in the energy variance, which also leads to a minimum in the energy. After a number of
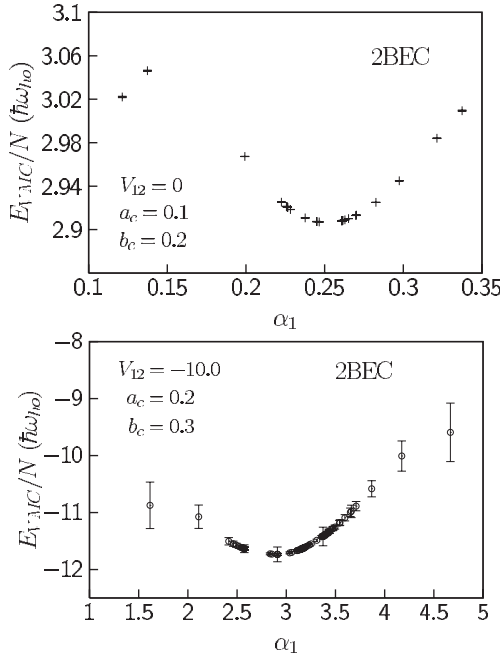
FIG. 2. VMC energy per particle versus the variational parameter α_1 of the trial wave function (3) for a trapped Bose gas mixture of $N_1=20$ and $N_2=10$ particles. Upper frame: HC 2BEC with $a_c=0.1$ and $b_c=0.2$. Lower frame: HCSW 2BEC with $a_c=0.2$, $b_c=0.3$, and $V_{12}=-10.0$. V_{12} is the interspecies HCSW depth.

iterations, we obtain plots such as those shown in the following figures. For example, Fig. 2 displays the VMC energy E_{VMC}/N versus one of the variational parameters α_1 for a mixture with $a_c=0.1$, $b_c=0.2$, and repulsive HC interactions only (upper frame) and for a mixture with $a_c=0.2$, $b_c=0.3$, attractive (HCSW, $V_{12}=-10.0$) interspecies and repulsive HC intraspecies interactions (lower frame). The figure depicts clearly the presence of energy minima at $\alpha_1 \sim 0.25$ and ~ 2.9, respectively. The behavior of the energy versus the other variational parameters is the same as in Fig. 2 and all of them display energy minima. After the completion of the optimization process and in the final evaluation of the wave function for each system, we choose the variational parameters that correspond to the energy minimum, i.e., the ground state. All of our repulsive or attractive 2BECs display energy minima as above and we can therefore state safely that our mixtures are stable systems.

In comparison, Fig. 3 shows the VMC energy against α for a HCSW 1BEC of 20 particles, HCSW depth $V=-6$ and $a_c=0.2$ using the same trial wave function (3) but set for one component only. The figure shows a peculiar result, namely, the presence of two equal energy minima at $\alpha \sim 1.15$ and 1.2, i.e., a degeneracy. One of the minima is due to the single-particle, the other due to the Jastrow part of the trial wave-function. The single-particle wave function is connected to the external trapping potential and the Jastrow function to the interparticle interactions and generates as such the energy minima due to these potentials. This plot has been generated from two VMC runs using different minimization directions [37] in order to ensure the presence of the two minima. We have seen this phenomenon in all the VMC runs for this particular system at various other HCSW depths. We do not
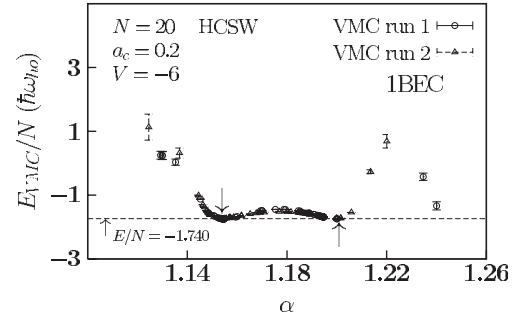

FIG. 3. As in Fig. 2 but for a HCSW 1BEC with $N=20$ particles. The depth of the HCSW is $V=-6$ and the arrows indicate the locations of two equal energy minima ($E/N=-1.740$). This plot is a result of two VMC runs of the same system.

understand at the present why this double minimum does not occur in 2BECs.

B. Definitions of the densities

In order to describe the density of the systems, we used na_c^3 with a_c the HS diameter of the bosons for component 1 and nb_c^3 with b_c the HS diameter for the bosons of component 2. We thus describe the systems by the HC density only, even in the presence of attractive interactions. We define the total VMC spacial density distributions (condensate +normal parts) by $n_1(r)$ and $n_2(r)$ for components 1 and 2, respectively, and in units of a_{ho}^3 where r is the distance of a boson of either species from the center of the trap ($r=0$). Correspondingly, $n_{0,1}(r)$ and $n_{0,2}(r)$ are the VMC condensate density distributions. The total VMC density of a 1BEC is written $n(r)$. In the interpretation of our results, we sometimes need to display the properties of both components as a function of their HC densities in a single plot. For this particular purpose, we use a unified term, namely, na_{HS}^3 with a_{HS} the HS diameter a_c or b_c, to describe the *HC* density of either component at the center of the trap and na_{HS}^3 is used then under the following conditions. In a single HC or HCSW 1BEC $na_{HS}^3=n(0)a_c^3$, where $n(0)$ is the number density at the center of the trap and a_c is the HC diameter of the single-species bosons. Since we are dealing with more than one species, na_{HS}^3 of each component has to be defined for various cases of interactions in the 2BECs. For systems with attractive interspecies interactions where there is full mixing (Sec. III C) $na_{HS}^3=n_1(0)a_c^3$ for component 1 and $na_{HS}^3=n_2(0)b_c^3$ for component 2. In the case of repulsive interspecies interactions na_{HS}^3 is the HC density of the core only since the two species phase separate (Secs. III D and III E) and it is difficult to define na_{HS}^3 for a shell. In all of our interpretations, we do not consider na_{HS}^3 to be the overall total density $[n_T(r)=n_1(r)+n_2(r)]$ of the mixture at any time.

C. Attractive interspecies and repulsive intraspecies interactions

1. Density profiles

The goal of this and the following sections is to display the spacial VMC density profiles of 2BECs with various in-
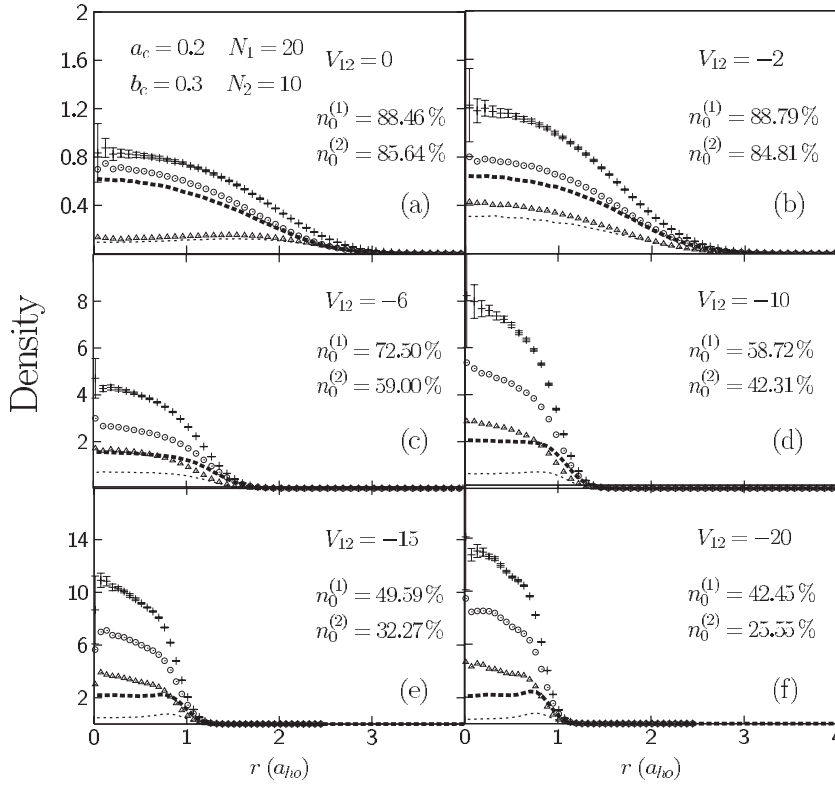
FIG. 4. VMC density profiles and condensate properties of 2BECs with HCSW interspecies and HC intraspecies interactions. V_{12} is the interspecies HCSW depth. Points with error bars: $n_T(r)$; open circles and triangles: $n_1(r)$ and $n_2(r)$, respectively; and thick and thin dashed lines: corresponding $n_{0,1}(r)$ and $n_{0,2}(r)$, respectively.

teraction parameters which have largely not been displayed before in the literature. Figure 4 displays the MC density profiles of 2BECs with attractive (HCSW) interspecies and repulsive (HC) intraspecies interactions. The points with error bars represent $n_T(r)$ of the mixture, the open circles represent the density $n_1(r)$, and the open triangles $n_2(r)$. The thick and thin dashed lines are $n_{0,1}(r)$ and $n_{0,2}(r)$, respectively. The strength of the interspecies interactions is indicated by the depth of the HCSW, $|V_{12}|$, and the range of the HCSW is kept fixed at 0.54. In all our mixtures, here and thereon, the components have $N_1=20$ and $N_2=10$ particles and in this section $a_c=0.2$ and $b_c=0.3$. There is a particular reason for the choice of the latter large a_c and b_c above; this is in order to enable substantial depletion of the condensates. We keep a_c and b_c fixed and increase V_{12} from 0 to −40 in the "negative" sense.

The key features of Fig. 4 are as follows. The attractive forces enable full mixing of the two components. In frame (a) component 2 is slightly pushed out towards the edges of the trap due to the repulsive interspecies interactions arising by setting $V_{12}=0$. That is, when the attractive part of the HCSW is switched off, the HCSW changes to a repulsive HC potential. Then we note that although $V_{12}=0$, full mixing of the two components is still possible. At the instant the HCSW is "switched on" as in frame (b), component 2 is *pulled back* towards the center of the trap with no remnant expulsion at the edges of the trap. The densities in frame (b) jump now above those in frame (a) and continue to rise as V_{12} is increased. In frames (a) and (b) the condensate densities $n_{0,1}(r)$ and $n_{0,2}(r)$ are similar in shape to their corresponding total densities $n_1(r)$ and $n_2(r)$, but in the rest of the frames (c)–(f) they are not. Rather they obtain a flat shape in frames (c) and (d) after which they are slightly pushed out

towards the edges of the trap in frames (e) and (f). In any case, the attractive forces prevent the condensate from total expulsion towards the edges of the trap. We anticipate that as the density rises further with V_{12}, the condensates will be pushed out further towards the surface of the cloud because the condensate seeks the lower density regimes of the cloud. The reason is because the lower cloud density at the edges of the trap causes a lesser local condensate depletion than the higher density towards the center. Note also that the total densities in frames (a)–(c) have a Gaussian shape, but then they divert from it somewhat. The densities rise also significantly with the increase of attractive interspecies interactions: $n_T(r)$ rises by a factor of ≈ 18 from frame (a) to frame (f) as the cloud radius shrinks in size by a factor of ≈ 3.

We are also able to use large attractive interspecies interactions ($V_{12}=-40$) at the energy scale of ultracold Bose gases and still obtain energetically stable systems.

2. Condensate fractions

The goal of this section is to display the effect of complete mixing on the depletion of each condensate in a 2BEC mixture as compared to the case when either condensate is in *a separate trap of its own* in which case it forms a 1BEC. For this purpose we consider the mixtures in Fig. 4. Figure 5 displays their condensate fractions as a function of na_{HS}^3. The open and solid squares represent the condensate fractions n_0 for HC 1BECs with $N=20$ and $N=10$ particles, respectively, which act as our *references*. The open and solid triangles display the condensate fractions of the mixtures $n_0^{(1)}$ and $n_0^{(2)}$. The figure depicts clearly that the depletion of the condensates in the 2BECs is larger than the 1BECs. This reveals that mixing enhances the depletions of the constituent condensates due to their interspecies interactions. A significant
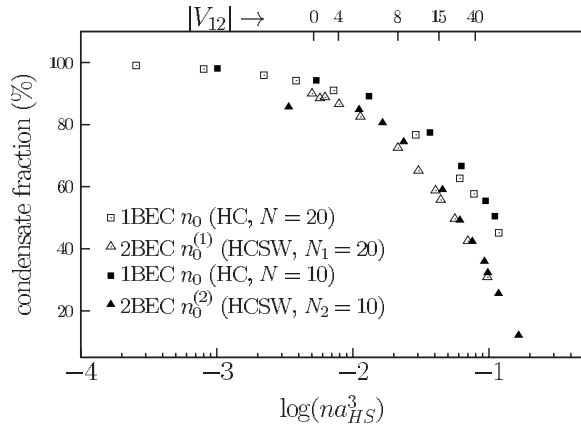
FIG. 5. Condensate fractions of HC 1BECs and the HCSW 2BEC of Fig. 4 as a function of na_{HS}^3. Open and solid squares: (reference) HC 1BECs with $N=20$ and $N=10$ particles, respectively. Open and solid triangles: components 1 and 2 of the HCSW 2BEC and V_{12} is the depth of the HCSW for some of the points. The points are larger than the error bars.

feature is that $n_0^{(1)}$ and $n_0^{(2)}$ as a function of na_{HS}^3 coincide at the larger na_{HS}^3. We may attribute this to the fact that since the two components are completely mixed the system behaves similarly to a 1BEC.

D. Attractive intraspecies and repulsive interspecies interactions

1. Density profiles

Figure 6 displays density profiles as in Fig. 4 but with $a_c=0.2$ and $b_c=0.4$ with HCSW intraspecies and HC interspecies interactions ($V_{12}=0$). We keep a_c and b_c fixed and vary the intraspecies HCSW depths $[V_{ii}, (i=1,2)]$ in the range $V_{ii}=-4$ to -16 keeping $V_{11}=V_{22}$. As a result of the attractive intraspecies interactions, the core and the shell contract in volume and the density of the system grows substantially in response from $n_T(0) \sim 2.5$ in frame (a) to ~ 14 in
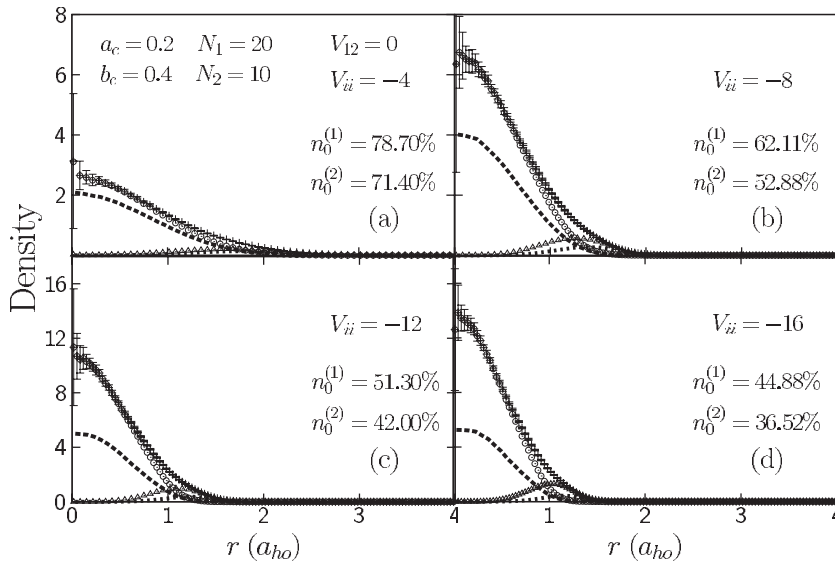

FIG. 6. As in Fig. 4 but with $a_c=0.2$, $b_c=0.4$ and HCSW intraspecies and HC interspecies interactions. The intraspecies HCSW depth is V_{ii} ($i=1,2$).
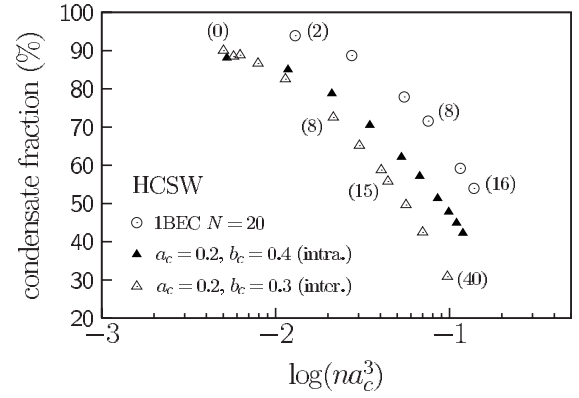

FIG. 7. Condensate fraction $n_0^{(1)}$ for HCSW 2BECs compared to a reference. Open circles: (reference) HCSW 1BEC with $N=20$ particles and $a_c=0.2$ in which the HCSW depth V is varied between 2 and 16. Solid triangles: 2BEC of Fig. 6 with attractive intraspecies interactions. Open triangles: 2BEC of Fig. 4 with attractive interspecies interactions. The numbers between brackets near to some of the points show $|V_{ij}|$ for the corresponding systems. The points are larger than the error bars.

(d) as the radius of the cloud shrinks from ~ 3 to 1.5. The shell is pushed radially inwards towards the center of the trap by the confining forces of the trap. Contrary to Fig. 4, the $n_{0,1}(r)$ and $n_{0,2}(r)$ profiles keep following the shape of their corresponding $n_1(r)$ and $n_2(r)$.

2. Condensate fractions

In what follows we investigate the condensate properties of 2BECs, this time with attractive intraspecies and repulsive interspecies interactions. This is somewhat the opposite case of Sec. III C where attractive interspecies and repulsive intraspecies interactions are used. We chiefly aim at revealing the difference in the results when using different types of combinations of repulsive and attractive interactions. Figure 7 compares now the condensate fraction $n_0^{(1)}$ of the 2BEC of Fig. 6 (solid triangles) with HCSW intraspecies interactions (intra.) against $n_0^{(1)}$ of the 2BEC of Fig. 4 (open triangles)
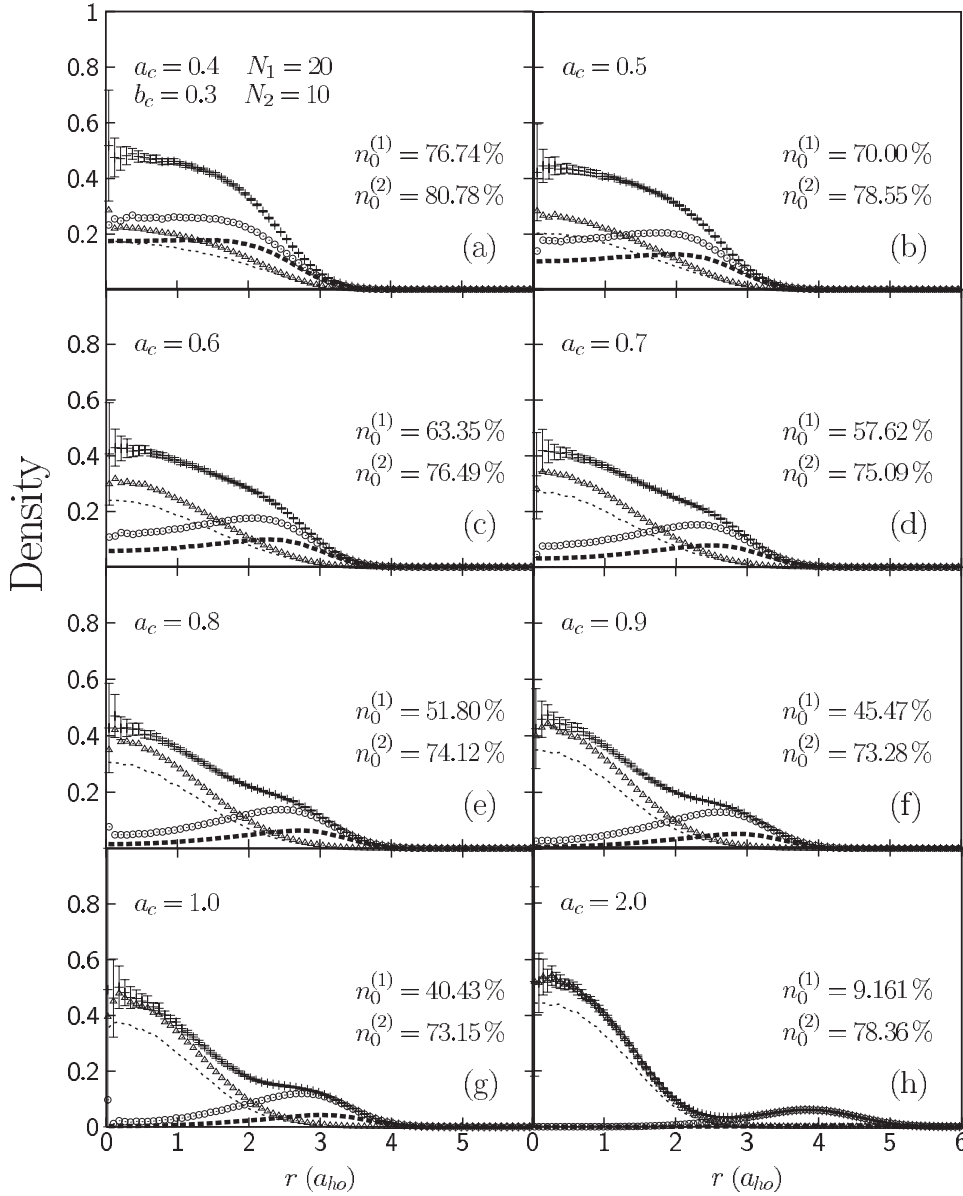
FIG. 8. As in Fig. 4 but with HC interactions only and varying a_c. b_c is held fixed at 0.3.

with HCSW interspecies interactions (inter.). The open circles display the condensate fraction n_0 of a HCSW 1BEC of $N=20$ particles and $a_c=0.2$ in a separate trap of its own; this is our *reference system*. Here the HCSW depth is varied in the range ($V=0$ to -16).

The condensate fraction $n_0^{(1)}$ of the mixture with attractive interspecies interactions (inter.) shows the largest depletion, although the bosons in its shell have a smaller HC diameter than those in the mixture with attractive intraspecies interactions (intra.). It seems that the attractive intraspecies interactions boost the value of the condensate (solid triangles) beyond the HC intraspecies result (open triangles). It will be shown in Sec. III E below that for a number of purely repulsive mixtures with the same bosonic HC diameters in the cores but different HC diameters in the shells, the condensate depletion is larger in the 2BECs with larger bosons in the shell. Our *reference* shows again the smallest condensate depletion, which is again a manifestation of the fact that mixing enhances the condensate depletion beyond the 1BEC result.

Substantial depletion is observed in Fig. 6 at $V_{ii}=-16$ ($\sim50\%$ for $n_0^{(1)}$ and $\sim60\%$ for $n_0^{(2)}$). If compared to Fig. 4 we can see that this amount of depletion sets in there at $V_{12}=-15$ (frame e), that is at a comparable (interspecies) HCSW depth. However, the density in the latter (~11) is lower than the former (~14) because the number of attracting pairs of two-species bosons is smaller in Fig. 4 than in our case here which leads to a slower rise in the density with HCSW depth.

E. Repulsive interspecies and intraspecies interactions

1. Density profiles

Figure 8 displays the VMC spacial density distributions of HC 2BECs with various interspecies interactions and the same definitions of points as in Fig. 4. Here a_c is varied while b_c is kept fixed at 0.3. We can see that mixing of the two components is enabled up to $a_c=1.0$ before complete phase separation sets in. On increasing a_c beyond b_c in frames (a)–(h), component 1 (of HC a_c) is gradually pushed
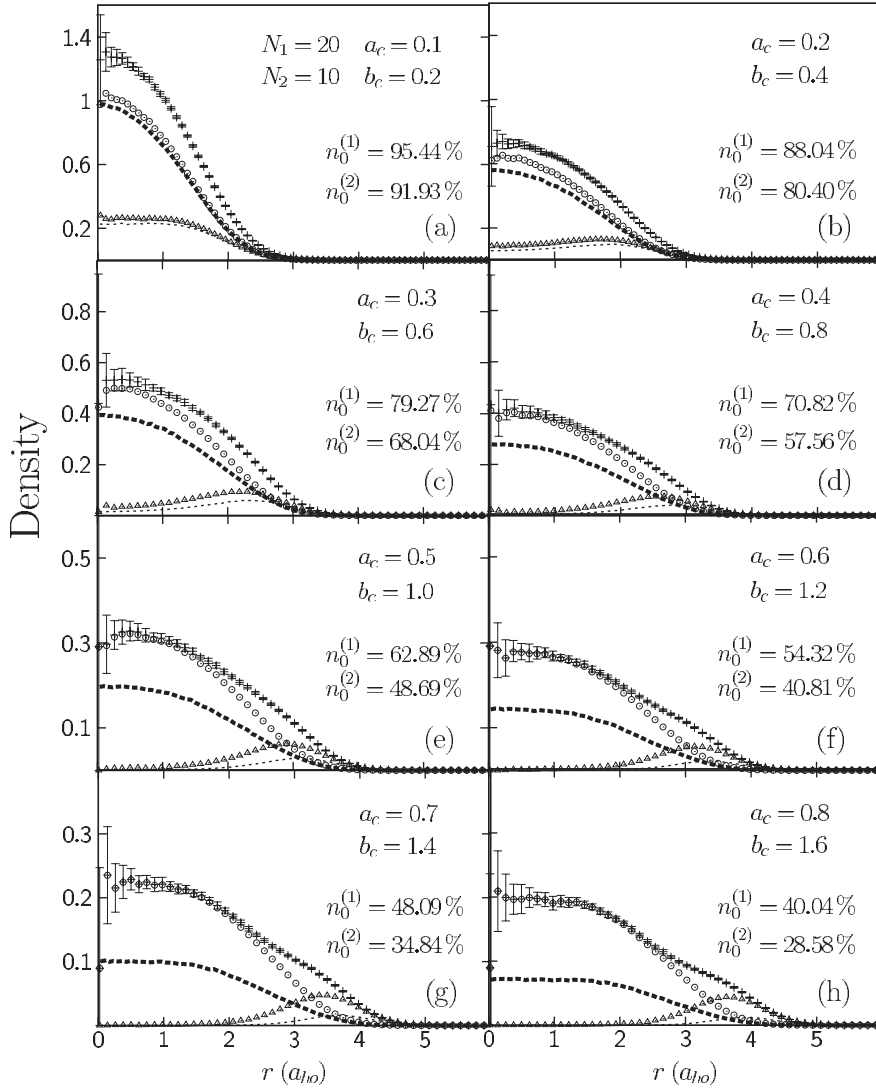
FIG. 9. As in Fig. 8 but with the HC diameters both varying at a fixed ratio of $a_c : b_c = 1 : 2$.

out towards the edges of the trap with the rise of interspecies repulsion $(a_c + b_c)/2$. This is contrary to our expectations because we thought that component 2 (of HC b_c) would be pushed out instead since it is the lighter of the two given that $m_1/m_2 = 1.200$ and $\omega_1 = \omega_2$. This can be explained as follows. Essentially, as the HC diameter of the bosons of one component increases, the Bose gas expands in size in order to accommodate the larger bosons. As a result, the component with lower intraspecies repulsion "falls" into the center of the trap seeking the minimization of the total repulsive potential energy. As the HC diameter a_c is increased, the interspecies repulsion rises pressurizing the core radially towards the center of the trap. As a result, the density of the core $n_2(0)$ rises by a factor of ≈ 2 from frame (a) to (h) and nearly as from frame (d) on, $n_1(0)$ begins to approach zero and the two components begin to separate into a shell and a core. If we imagined removing the shell completely from the trap, the core will expand and become almost uniform in density and therefore "flat" in shape [33,34]. We found that it is very hard to "squeeze" the core further to higher density by increasing a_c beyond 2. In frame (h) total phase separation has occurred leaving a dip at the boundary between the two components. One could imagine placing a third-species particle

in that dip as it is a potential trap by itself. Contrary to the case of Figs. 4(d)–4(f), the condensate density distributions of both components follow the shape of their total densities up to phase separation.

With repulsive interactions only in these mixtures, we can always have stable systems if there is sufficient repulsion between the bosons of the core counteracting the outer pressure arising from the shell. Otherwise a dilute core collapses readily under the heavy pressure of a dense shell.

Figure 9 displays the MC density distributions of a 2BEC with HC interactions only where a_c and b_c are both increased at a fixed ratio $a_c : b_c = 1 : 2$. In this case the density of the core $n_1(0)$ decreases because both a_c and b_c are increased. A peculiar result is that even at very large values of the interspecies repulsions no complete phase separation is observed as it occurs in Fig. 8(h). Some uniformity in the density distribution of the core arises at the larger a_c.

In Fig. 10 we make comparisons between densities at the center of the trap as a function of the interaction parameter $N_1 a_c$ for various systems with repulsive interactions. The crosses are for a HC 1BEC of 20 particles *in a separate trap of its own* and the same trap length as before $a_{ho} = \sqrt{\hbar/m_1\omega_1}$. The open circles and triangles are, respectively,
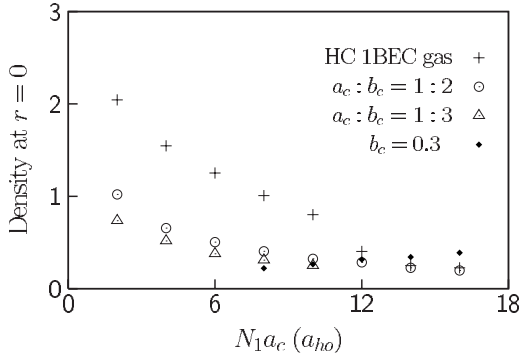
FIG. 10. Density at the center of the trap ($r=0$) vs the interaction parameter $N_1 a_c$ for HC systems only. Crosses: 1BEC with $N=20$ particles (reference); open circles: 2BEC of Fig. 9 with $a_c:b_c=1:2$; and open triangles: 2BEC with $a_c:b_c=1:3$; solid diamonds: 2BEC with b_c fixed and a_c varying (Fig. 8). The points are larger than the error bars.

for the core in Fig. 9 and an additional mixture with $a_c:b_c=1:3$ whose density profiles we do not reveal. The solid diamonds are for the core in Fig. 8. Thus the goal is to show the effect of mixing a HC 1BEC with various other 1BECs on the central core density of the system. The density $n(0)$ of the HC 1BEC drops as it is mixed with another component, and for a larger ratio of b_c relative to a_c the core density drops further. The density of the core with one of the HCs fixed ($b_c=0.3$) varies only slightly as a_c increases. Note that the values of the core density at $r=0$, except for the latter case, converge at the higher $N_1 a_c$.

2. Condensate fraction

Figure 11 compares the condensate fraction $n_0^{(2)}$ of Fig. 8 ($a_c:b_c=1:2$) to two other systems. The open circles display n_0 for a HC 1BEC of ten particles *in a separate trap of its own* and the same trap length as before $a_{ho}=\sqrt{\hbar/m_1\omega_1}$. The solid triangles display $n_0^{(2)}$ for the HC 2BEC of Fig. 8 with b_c fixed and a_c varying. The open triangles display $n_0^{(2)}$ for the HCSW 2BEC of Fig. 4 with a_c and b_c fixed and V_{12} varying. We note that the condensate depletion is highest in the HC 2BEC of Fig. 8. The depletion of the condensate in the
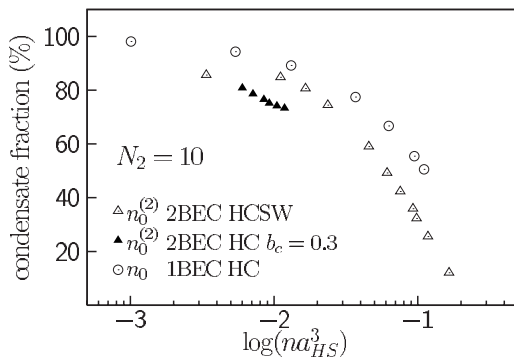

FIG. 11. Condensate fraction vs na_{HS}^3 for a HC 1BEC and component 2 in 2BECs. Open triangles: HCSW 2BEC of Fig. 4; solid triangles: HC 2BEC of Fig. 8; and open circles: HC 1BEC with $N=10$ particles (reference). The points are larger than the error bars.
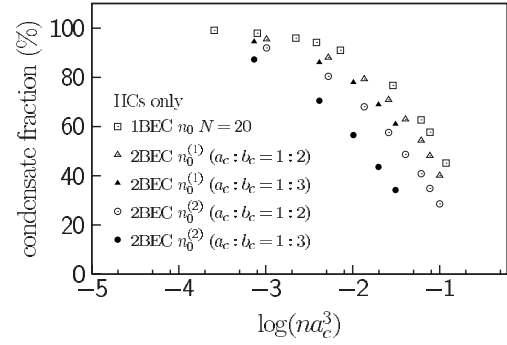

FIG. 12. Condensate fraction vs na_{HS}^3 for HC systems only. Open squares: 1BEC of $N=20$ particles; open triangles and circles: $n_0^{(1)}$ and $n_0^{(2)}$ for the 2BEC of Fig. 9; and solid triangles and circles: $n_0^{(1)}$ and $n_0^{(2)}$ for a HC 2BEC with $a_c:b_c=1:3$. The points are larger than the error bars.

HCSW 2BEC is less pronounced. This reveals that the repulsive interspecies interactions play a more pronounced role in depleting the condensates of the mixture than attractive interspecies interactions. The attractive interspecies interactions boost the condensate somewhat above the HC-interspecies interactions result. The depletion of the condensate is lowest for a 1BEC. Thus the mixing of condensates enhances their depletion due to the presence of interspecies interactions of various strengths as compared to the case when they are separate, each in a trap of its own.

Figure 12 displays chiefly the condensate fractions of the components as a function of na_c^3 at the center of the trap in various HC systems compared to a *reference*. The open squares represent the condensate fraction n_0 of a HC 1BEC of 20 particles (reference). The open triangles represent the condensate fraction $n_0^{(1)}$ of the 2BEC of Fig. 9 where a_c and b_c are varied at a constant ratio of 1:2 and the solid triangles that at a ratio of 1:3, respectively. In addition, and for further comparison, the open and solid circles represent $n_0^{(2)}$ of the latter two mixtures, respectively. We can see that $n_0^{(1)}$ is lower for $a_c:b_c=1:3$ than for 1:2 and the same is true for $n_0^{(2)}$. The latter values of $n_0^{(1)}$ are lower than those of the HC 1BEC displayed for comparison. This shows again that mixing and a larger interspecies interaction enhance the depletion of the condensates in each component beyond the 1BEC result.

F. Energies

In this section we compare our VMC energies for HC 2BECs against the energies calculated by an approximate model derived from mean-field results in Appendix A. The estimate that we obtained for the total energy of the mixture E^{MFA} is given by Eq. (A10) where MFA stands for mean-field approximation.

Figure 13 displays our VMC energies for the repulsive mixtures investigated in Fig. 9 with $a_c:b_c=1:2$ (open triangles) and 8 with $b_c=0.3$ (solid circles). The open diamonds show the additional VMC calculations for HC 2BECs with $a_c:b_c=1:3$ similar to Fig. 9. The crosses, times, and open circles display E^{MFA} for the systems indicated by the open triangles, diamonds, and solid circles, respectively. We note
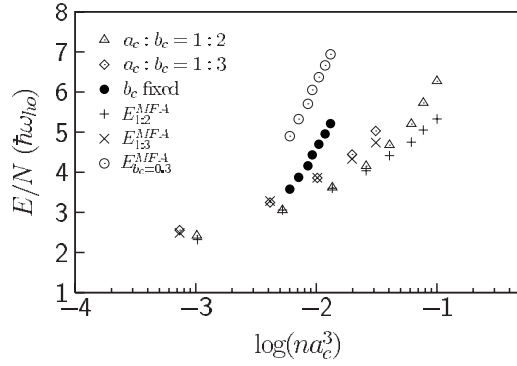
FIG. 13. VMC energies and energies of Eq. (A10) (E^{MFA}/N) vs the HC density na_{HS}^3. Open triangles: mixture in Fig. 9 ($a_c:b_c$ =1:2); open diamonds: the mixture with $a_c:b_c$=1:3; and solid circles: mixture in Fig. 8 (b_c=0.3). Crosses, times, and open circles: corresponding estimates E^{MFA}/N in the same order. The points are larger than the error bars.

that there is good agreement between the energies $E_{1:2}^{MFA}$ and the VMC results at the lower na_c^3 but then they begin to diverge somewhat at the higher densities. The same is true for $E_{1:3}^{MFA}$. $E_{b_c=0.3}^{MFA}$ largely do not agree with the VMC results but show the same trend in their values. This might be chiefly due to the fact that the TF radius of the core is not a good representation of the cloud radius for this particular case because the two components completely phase separate at the higher interspecies repulsions. In all cases, the energies rise with the HC densities. The rise is steepest when b_c is fixed and a_c varied, the reason being due to the fact that the core density varies slowly with the rise of a_c (see Fig. 8). That is, as the shell is expelled towards the edges of the trap, the potential energy rises faster than the change in $n_2(0)b_c^3$ compared to the other systems.

G. Effect of mass ratio

In this section we present the role of the mass ratio $m_{ratio}=m_1/m_2$ in determining the properties of mixed Bose gases. We consider two mass ratios, the previous $m_{ratio}=1.2$ and a new $m_{ratio}=5$ and in order to keep the trap length
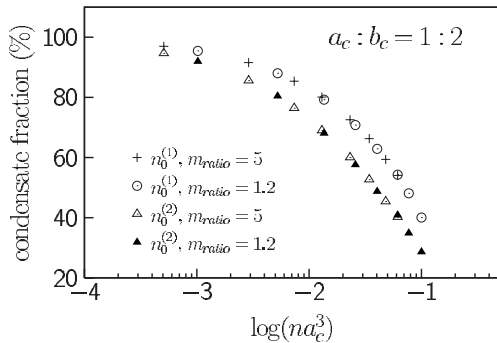

FIG. 14. Condensate fractions vs na_{HS}^3 for two mass ratios of a HC 2BEC with $a_c:b_c$=1:2. Crosses and open circles: $n_0^{(1)}$ for m_{ratio}=5 and 1.2, respectively, open and solid triangles: $n_0^{(2)}$. The points are larger than the error bars.
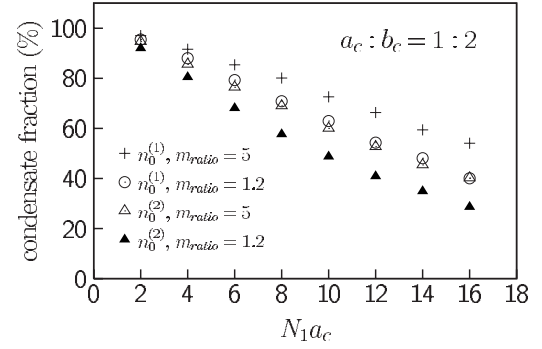

FIG. 15. As in Fig. 14 but vs N_1a_c instead of na_{HS}^3. The points are larger than the error bars.

unchanged, we only change m_2. We further note that changing m_{ratio} changes the energy of the system since m_1/m_2 and m_2/m_1 appear explicitly in the Hamiltonian (2).

We consider the systems depicted in Fig. 9 with m_{ratio} =1.2 and compare its properties with those of exactly these same systems evaluated at m_{ratio}=5.0. Figure 14 displays the condensate fractions of the latter systems versus na_c^3, where the condensate fraction $n_0^{(1)}$ (and $n_0^{(2)}$) is the same for both values of m_{ratio}. Therefore m_{ratio} has no influence on the relation between condensate fraction and HC density. The scenario is, however, different if one plots the condensate fractions as a function of the HC interaction parameter N_1a_c as in Fig. 15. The crosses and open circles show $n_0^{(1)}$ and the open and solid triangles $n_0^{(2)}$ each for m_{ratio}=5 and 1.2, respectively. We can see that the condensate fractions for m_{ratio}=5 are higher than for 1.2 because the central HC densities are lower for 5. Effectively, as m_2 is reduced to increase m_{ratio}, the trapping forces confining the shell ($-\nabla\frac{1}{2}m_2\omega^2r_2^2$) are reduced accordingly. Thus, the cloud of the mixture expands as the pressure of the shell on the core is lifted causing the central densities to decline in favor of an increase of the condensate fractions. Figure 16 displays na_c^3 as a function of N_1a_c for the latter systems where na_c^3 for m_{ratio}=5 is lower than for 1.2 at higher N_1a_c as explained above. As we increase m_{ratio}, the energy of the system rises as demonstrated in Fig. 17, where E_{VMC}/N is plotted against na_c^3 for two m_{ratio} values and $a_c:b_c$=1:2.

IV. DISCUSSION

We discuss now important details on the results of our calculations and connect to the previous literature. We elabo-
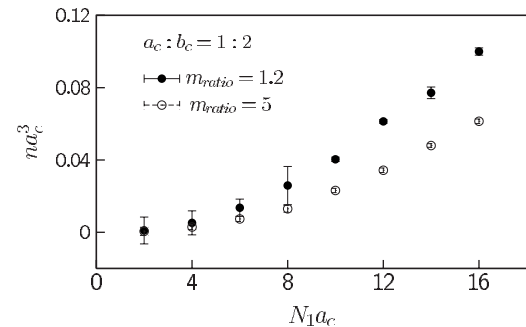

FIG. 16. na_c^3 as a function of the interaction parameter N_1a_c for two mass ratios of a HC 2BEC with $a_c:b_c$=1:2.
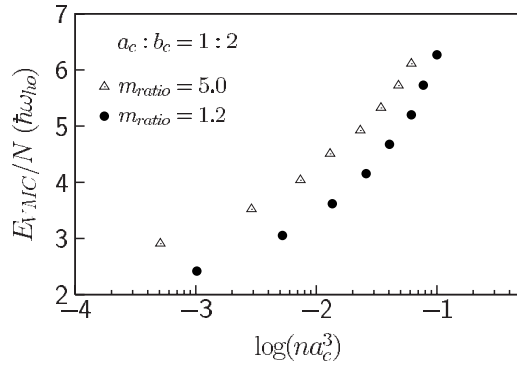
FIG. 17. VMC energy for the same systems in Fig. 16 and two mass ratios. The points are larger than the error bars.

rate on the mixing and phase separation of components, stability of the mixtures, and the origins of the enhanced condensate depletion. First of all, however, we mention briefly the work of Ma and Pang [17], which is most relevant to ours.

A. Work of Ma and Pang

Ma and Pang [17] investigated HC 2BECs trapped in a three-dimensional isotropic trap at finite temperature using path-integral quantum Monte Carlo simulations. Their main interest was in the structure of the mixtures, i.e., the densities and their profiles. They particularly concentrated on the conditions under which phase separation occurs and treated the two-species system as two subsystems each of which contains one species with its own statistics. However, the two species do not behave independently of each other due to the interspecies interactions. They found that by changing the mass ratio of the components m_2/m_1 the lighter particles are pushed outward and form a shell surrounding the heavier core. Further, the density and condensate fractions of the mixture drop with a rise of the interspecies interactions. When identical external potentials are used, no phase separation is observed, but when they are different, phase separation occurs. They also found that the spacial phase separation is independent of m_2/m_1 and that the species with the larger scattering length favors the formation of a low-density outer shell.

Now in our work here we conducted our calculations at zero temperature and we simulated two-species Bose gases with both attractive and repulsive interactions. We particularly concentrated on the role of the interspecies and intraspecies interactions on the enhancement of the condensate depletions in the mixture as compared to the case when each component is in a separate trap of its own. We followed Ma and Pang in treating each component as a subsystem with its own properties. In addition to their investigations on the effect of the mass ratio, we additionally investigated its effect on the energies and condensate fractions.

B. Mixing and demixing

In the case of intercomponent attraction as in Fig. 4 no phase separation occurs because the two gases attract each other. Note that the attractive interspecies interactions at some point overwhelm the repulsive intraspecies interactions as identified by the large increase in the overall density $n_T(r)$ of the system. That is, the repulsive intraspecies interactions do not become attractive, they just get overwhelmed similar to a case discussed by Chui and Ryzhov [38]. Further, the two gases are now trapped by the attractive potential of each other such that the importance of the external trap is underplayed. Since in all our calculations the minima of the two confining potentials coincide, the two components interpenetrate completely [12] and are drawn together into what resembles a 1BEC system acting similarly to it. We conclude that in this case, the attractive interspecies interactions play a more pronounced role than the repulsive ones in determining the properties of the systems. Therefore the condensates are able to migrate towards the edges of the trap at the higher densities na_{HS}^3 as in the case of a HC 1BEC [33]. In the somewhat opposite case of Fig. 6 the intercomponent repulsion pushes the condensate of the core towards the center of the trap.

In the case of Figs. 8 and 9, we find chiefly that full mixing is impossible at large repulsive interspecies interactions. Larger interspecies repulsion leads to full phase separation as in Fig. 8(h) and even though the shell there has a much lower density than the core, substantial depletion $\sim 20\%$ is still observed which is attributed to the presence of large bosons in the shell. Note that it is hard to define a density na_{HS}^3 for the shell as it is expelled towards the edges of the trap.

An investigation of the detailed nature of the overlap region between the shell and core is also important since it influences properties such as the ground state energy, the excitation spectrum, and the collisional relaxation rates as outlined earlier by Barankov [11]. He explored the boundary between two repulsively interacting condensates in the weak and strong separation limits and found that the asymptotic behavior of each condensate far from the boundary is determined by its correlation (healing) length. In the case of strong separation, he found that there exists a hollow in the total density profile which is very deep. The latter allows the investigation of one-particle excitations at the boundary between the components as well as surface wave excitations due to the surface tension [11]. As a result of the full separation in Fig. 8, we also observe a hollow in the total density profile between shell and core as discussed by Barankov. In the future one could add *one* foreign particle to be trapped by this hollow and investigate its energy as a function of some property of the mixture using the Monte Carlo method. Such a hollow is, however, not observed in Fig. 9 because no complete phase separation occurs. The reason is because as the HC diameters of the bosons in the core are increased, the bosons spread out and the core expands. As a result, these bosons penetrate into the shell which is pushed in the opposite direction towards the center of the trap by the confining forces of the external potential. This is, however, not the case in Fig. 8 as the HC diameters of the bosons in the core are kept fixed and that of the shell increased. Thus complete phase separation is only possible when the size of the bosons in only one component is increased. This has also been confirmed by Ma and Pang previously.

Two length scales can be used to characterize a two-component BEC [16]: one is the penetration depth, the other is the healing length. The penetration depth is a measure for the width of the overlap region and, as we can see from above, a function of the interspecies interactions. It is largest in the case of attraction between the two components as it is equal to the radius of the cloud whereas in the case of large intercomponent repulsion it is smaller than the radius of the cloud. The penetration depth is reduced as the intercomponent repulsion rises. Nevertheless, complete mixing is still possible at moderate repulsive interspecies forces as demonstrated in Figs. 8 and 9. Since the density profile of the core in the latter two systems is very much influenced by the presence of a shell, we anticipate that the healing length of a 1BEC changes upon mixing with a shell. In what follows, we discuss some of the previous literature in connection to our current observations.

Shchesnovich *et al.* [4] studied a ^{85}Rb and ^{87}Rb 2BEC by varying the interspecies interactions. They found that these two components would not separate if the interspecies interactions are attractive and in this paper we have verified this point as well. They argued that a separation of the two species takes place when the energy gain due to the attractive intraspecies interactions overwhelms the quantum pressure at the interface of the two species.

Cornell *et al.* [12] reviewed some early results on mixed condensates and provided a qualitative exegesis of the theoretical and experimental techniques that are involved. They found that there is a critical value for the interaction term $a_{12}^c = \sqrt{a_1 a_2}$ beyond which phase separation occurs with little spatial overlap. This is when the scattering length a_1 of component 1 becomes larger than a_2 of component 2, causing atoms 1 to move favorably towards the edges of the cloud forming a spherical shell around the core consisting of atoms 2. Our results are in line with those of Cornell *et al.* [12] and also Hall *et al.* [14] as we also observe that the component with the larger bosonic hard-core diameter migrates to the edges of the trap.

Shi *et al.* [10] studied the phase separation of two-species trapped and untrapped Bose gases at finite temperature and found that the interspecies interactions affect the formation and depletion of the two condensates and lead to spatial phase separation of the mixture. They argued that the shell is trapped in an effective potential which has a minimum away from the center of the trap close to the surface of the core. This effective trap is a combination of the traps confining the mixture and the interspecies interactions. According to Shi *et al.* then, condensation of the shell happens at the surface of the core and indeed we do observe a condensate in the shell as displayed in Figs. 8 and 9.

C. Why do we use a HCSW?

Particularly, the HCSW is a suitable potential to describe the attractive interactions between the HS bosons in this work, since it is a HC contact interaction plus an attractive tail added to the HC and the HC diameter is the same as the HS diameter of the bosons. Another reason for choosing the HCSW is to simulate a Feshbach resonance. This is because

the HCSW has a well defined range, width, and depth and via these parameters one can easily tune the scattering length to be at the Feshbach resonance using Eq. (11) below when $a \to \pm \infty$ in order to check any instabilities (or stabilities) arising from this. In terms of designing the trial wave function, the exact solution of the two-body Schrödinger equation interacting via a HCSW led us in the construction of a flexible Jastrow function for HS bosons with attractive interactions as mentioned in Sec. II D.

D. HCSW parameters used

Our main purpose for the choices of the previous values of the HCSW parameters in this work was to provide a qualitative study of the properties of trapped Bose-gas mixtures with attractive interactions and to reach a qualitative understanding of the role of the interatomic interactions in these properties. We first remind the reader that the values of the HC diameters have been chosen to enable substantial depletion of the condensate.

1. Range

The range of the HCSW ($d = 0.54 a_{ho}$) used in this work is of the same order of magnitude as that used by Astrakharchik *et al.* [35] for another model potential of the form $V(r) = -V_0 / \cosh^2(r/r_0)$. Here r_0 determines the range and they set $r_0 = 0.1 a_\rho$, where a_ρ is the transverse oscillatory trap length for a highly elongated trap. Their a_ρ is small because of tight confinement along the transverse direction; similarly our a_{ho} is also considered to be small since we use a tight trap.

2. Depth

We use a shallow HCSW which is much weaker than a realistic interatomic potential [39,40], drawing our justification from what has been noted before by Gao [41]. He discussed improved interatomic model interactions beyond the HS potential or delta function pseudopotential used in Gross-Pitaevskii theory. These model potentials are simple in a sense that they are shallow and are applicable in quantum few-body and many-body systems.

One of the most important points relevant to our work mentioned by Gao is that a real interatomic potential can simply become unmanageable if used in few-body or many-body calculations. A key conclusion in his paper is that the real potential in a many-body system around the threshold, such as a BEC state, no matter how deep this potential might be, can be replaced by an effective shallow potential that supports only one or two bound states. Gao shows that by using shallow model potentials, much weaker than the real potentials, the results are in good agreement with those using a real interatomic potential.

E. Artificial stability of the mixtures, Feshbach resonance, and negative energies

1. Artificial stability with large HCs

The large HC potentials used in this investigation, whether attractive or repulsive, prevent real collapse and therefore the mixtures are always stable and cannot collapse
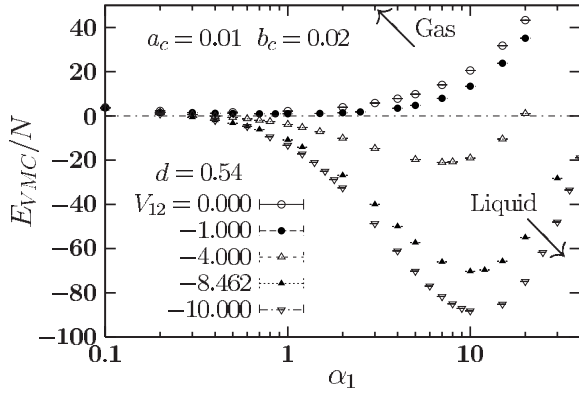
FIG. 18. Energy vs α_1 showing stabilities at high HCSW depths for a two-component Bose gas of $N_1=20$ and $N_2=10$ particles, $a_c=0.01$, $b_c=0.02$, $d=0.54$ and various interspecies HCSW depths V_{12} shown. The first Feshbach resonance for the system is at $V_{12}=-8.462$.

to a singularity in this case. In that sense, we speak of an "artificial stability" [42]. This HC is present in the HCSW potential since upon "switching on" a HCSW one effectively adds to the HC potential an attractive tail, well defined in width and depth. Thus, whatever the depth of the HCSW is, the bosons will not be able to approach each other to distances lesser than the HC diameter of the interactions [a_c, b_c, or $(a_c+b_c)/2$] as imposed by the Jastrow functions. As mentioned in Sec. II D, the Jastrow function of the HCSW has a short-range repulsive and a long-range attractive part. The short-range part of the HCSW Jastrow keeps the bosons at some average distance away from each other, whereas the attractive part tries to bring them closer together. The balance between the repulsive and attractive parts, keeps the system in equilibrium. In the case of repulsive interactions only, the system is primarily balanced by the repulsive HC and the external confining potential.

2. Feshbach resonance with large HC diameters

Using the present model potential with *large* HC diameters of the order of 10^{-2} does not reproduce the predicted phase transition at exactly the Feshbach resonance as it does with small HC diameters (see Sec. IV E 3). That is, the model potential with large HCs does not show that the HCSW Bose gas loses its stability at the parameters of the model potential corresponding to a Feshbach resonance scattering length. This is the stability which a dilute Bose gas with small HCs has at potential parameters just before the Feshbach resonance. We shall return to this point shortly below.

Henceforth if one should increase the HCSW depths to values up to the first Feshbach resonance and beyond, the systems begin to shrink to very high densities. At this stage their energy is mainly potential (negative) and a large fraction of the bosons reside inside the HCSW. However, they still show the artificial stability discussed above at large α values. For example, in Fig. 18 we demonstrate how the stability of a two-species HCSW Bose gas of $N_1=20$ and $N_2=10$ particles with repulsive HC intraspecies interactions,

$d=0.54$, and HS diameters $a_c=0.01$, $b_c=0.02$, respectively, shifts to higher α values as V_{12} is increased from shallow to deep values, even up to the first Feshbach resonance at $V_{12}=-8.462$ and beyond. The HCSW depth corresponding to a Feshbach resonance is obtained from the condition that $a \rightarrow \pm \infty$, where a is the s-wave scattering length of the HCSW. And according to Giorgini *et al.* [43] a is given by

$$a = R_c + (R - R_c)\left\{1 - \frac{\tan[K_0(R - R_c)]}{K_0(R - R_c)}\right\}, \quad (11)$$

where R_c is the HC diameter (in our case a_c for component 1, b_c for component 2, or $(a_c+b_c)/2$ for the mixture), R is the edge, and $K_0=\sqrt{V_0 m/\hbar^2}$ is the wave vector of the HCSW. In trap units $R_c \rightarrow R_c/a_{ho}=\widetilde{R}_c$ and similarly for R, $V_0 \rightarrow V_0/\hbar\omega_{ho}=\widetilde{V}_0$, and thus $K_0 \rightarrow \sqrt{\widetilde{V}_0 \hbar\omega_{ho} m/\hbar^2}=\sqrt{\widetilde{V}_0}/a_{ho}=\widetilde{K}_0$.

In Fig. 18 at $V_{12}=-10$ the wave function is very much contracted and its density has risen substantially as indicated by a large Gaussian variational parameter ~ 10. Note that one still obtains a deep negative energy minimum at the first Feshbach resonance manifesting the strong stabilizing factor of the HCs. Thus even if we reach the Feshbach resonance and surpass it while varying the HCSW depth, the systems remain artificially stable. Going back to the previous Fig. 4, for example, we crossed a Feshbach resonance while increasing V, but no sharp density profile indicative of a collapse can be seen. In Sec. IV E 4, we shall explain the occurrence of the negative energies to be the result of a liquefaction process of the Bose gas since when the energy becomes negative, energy is released from the system. Thus, with large HC diameters on the one hand, one cannot show that the Bose gases lose their stability at exactly the Feshbach resonance. On the other hand, with small HC diameters this is possible as explained in the next section.

3. Feshbach resonance with small HC diameters

By using small HC diameters we demonstrate that the present VMC method with a HCSW potential is able to detect a phase transition at exactly the Feshbach resonance. For this purpose we consider here a different approach in which we fix the depth of the HCSW V_0 and its HS diameter a_{HS} and vary its range d under the condition that $a_{HS} \ll a_{ho}$ and $d=R-a_{HS} \ll 1$. We consider henceforth a dilute Bose gas with—for instance—$N=40$ particles, $a_{HS}=1.0 \times 10^{-6}$, and $V_0=986.960$ corresponding to a Feshbach resonance at $d=0.05$. We vary the range of the HCSW from 0.001 to 0.06 essentially passing through the first Feshbach resonance for V_0 above at $d=0.05$, where the scattering length $a \rightarrow +\infty$. Figure 19 shows the energy versus the main variational parameter α for the latter system at various ranges d. There we have $d=1.0 \times 10^{-3}$ [$a=+6.71 \times 10^{-7}$, open squares (with error bars)], 0.03 ($a=-1.38 \times 10^{-2}$, open triangles), 0.04 ($a=-5.80 \times 10^{-2}$, open diamonds), 0.05 ($a \rightarrow +\infty$, with solid diamonds) at the first Feshbach resonance, and 0.06 ($a=+1.58 \times 10^{-1}$, half-filled circles beyond the first Feshbach resonance). The system is stable for d up to 0.04 where there is still an energy minimum at $\alpha \sim 1$ indicated by an arrow. For $d=0.05$ corresponding exactly to the Feshbach resonance for the above HCSW depth, the system loses its earlier stability
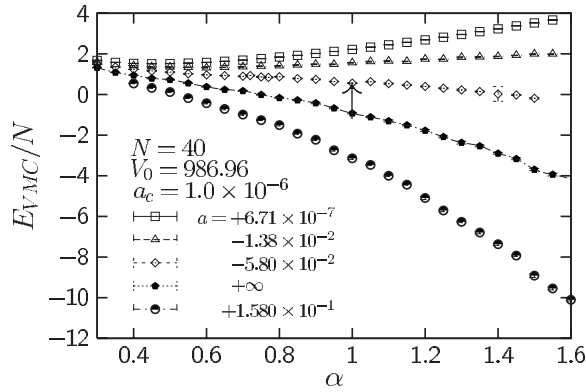
FIG. 19. VMC energy vs the main variational parameter α showing the vanishing stability of a HCSW Bose gas of $N=40$ particles, HS diameter $a_{HS}=1.0\times10^{-6}$, and well depth $V_0 =986.960$ as the HCSW range d is increased starting from a value corresponding to a stable HCSW Bose gas while keeping V_0 fixed. The chosen well depth corresponds to a Feshbach resonance at a HCSW width of $d=0.05$. Open squares: $d=1\times10^{-3}$ corresponding to $a=+6.71\times10^{-7}$; open triangles: $d=0.03$, $a=-1.38\times10^{-2}$; open diamonds: $d=0.04$, $a=-5.80\times10^{-2}$; solid diamonds: $d=0.05$ at the Feshbach resonance $a=+\infty$; and finally, the half-solid circles are for $d=0.06$ corresponding to $a=0.158$. Energies and lengths are in trap units.

which it had at potential parameters just before the onset of the first Feshbach resonance. On increasing the HCSW depth, we anticipate that the Bose gas will shrink to higher densities and reach it highest compression at a very high α value. Figure 19 gives qualitatively similar results to Fig. 3 of Ref. [35] where it is clearly seen that the energy barrier stabilizing their system vanishes with the decrease of their Gaussian width. We must note that in our case α corresponds to the inverse of the Gaussian width. Thus with small HC diameters in the dilute regime, the HCSW potential is able to reproduce the loss of stability of a trapped Bose gas at exactly the Feshbach resonance.

4. Liquefaction of Bose gases (negative energies)

The bosons can condensate to a dense liquid at critical values of the scattering length and potential depth. This is signified by the occurrence of negative energies as in Figs. 2, 3, and 18. The liquid density is set by the range of the attractive well since there is a large energy incentive for a boson to lie in the attractive well of its neighbors but no further potential energy incentive to lie closer than that. There is a cost in kinetic energy increase if the bosons move closer together. Thus the density of the liquid saturates eventually to a value set by the range of the HCSW (and less so by the HC diameter).

There is a large energy release on condensation of the Bose gas to the dense liquid state. In Fig. 18 we show how the energy drops from $E/N\approx1.6$ at $V_{12}=0$ to $E/N\approx-90$ at $V_{12}=-10.0$. Thus energy is released at a degree that is proportional to the well depth V. Upon condensation, there is substantial depletion of the condensate so that a large percentage of the atoms lie in states above the condensate. Thus the condensation process is characterized by a large increase

in the density of the system, a large drop in the energy of the system until there is a large release of condensation, and a substantial depletion of the condensate.

F. Condensate depletion

In this section we explore possible reasons for the enhanced depletion of the condensates in the mixtures. We believe that due to mixing the reduction in free volume between the HS bosons available for condensate formation in each species is a common ground for enhanced depletion in all types of mixtures. The magnitude of reduction in free volume varies, however, with the types and strengths of interactions. As the free volume between the HS bosons decreases, the probability for relocating a boson at a certain site, say $\mathbf{r}_1$ and energy ϵ_0 to another location at $\mathbf{r}_1'$ and the same energy ϵ_0 is reduced. This is because the chance of finding a site between the bosons large enough to accommodate a boson becomes lower.

Going back to Fig. 7 then, the reason the mixtures with interspecies attraction (of Fig. 4) indicated by (inter.) show a larger depletion for component 1 (with HC a_c) than the mixtures with interspecies repulsion (of Fig. 6) indicated by (intra.) is because the former are completely mixed as compared to partial mixing of the latter. In the case of complete mixing the available volume for condensate formation is severely reduced and smaller than the case of partial mixing. Further, since both components in Fig. 4 are localized at the center of the trap, they contribute to their mutual condensate depletion where the density is highest, namely, at the center of the trap. In the case of partial mixing the shell contributes to the depletion chiefly at the edges of the trap and does not influence the condensate at the center of the trap very much. There could also be other reasons that explain the enhancement in the depletion.

The scenario is, however, different for component 2. In Fig. 11 the depletion is larger for the 2BEC with interspecies repulsion (of Fig. 8) than the 2BEC with interspecies attraction (of Fig. 4). The reason may be because the boson sizes a_c of the HC 2BEC are increased far above those of the HCSW 2BEC which remain fixed thus outweighing the role of the HCSW in the depletion (free-volume reduction).

G. Ground state solutions

Trippenbach et al. [16] identified all possible classes of solutions for 2BECs and found that, in the case of isotropic harmonic trapping potentials, many spherically symmetric phase-separated geometries are possible. In addition, symmetry breaking solutions do exist but within the TF approximation the ground state cannot be one with broken symmetry. Similarly, our mixtures are spherically symmetric in their ground states.

V. CONCLUSIONS

In summary then, we have investigated the effect of intraspecies and interspecies interactions on the properties of ultracold 2BECs in tight harmonic traps using VMC. The repulsive interspecies or intraspecies interactions were mod-

eled by a HC contact potential, the radius of which is being equivalent to the *s*-wave scattering length in the low-energy and long-wavelength approximation. The attractive interactions were modeled by a HC repulsive part plus a shallow attractive well, the HCSW. We did not describe the attractive interactions by the HCSW scattering length *a*, but rather the depth of the HCSW in order to avoid the large fluctuations in the value of *a*. We calculated the energies, density distributions, and condensate density distributions. We further obtained the condensate fractions of the components from the OBDMs. A key point is that we chiefly focused on the role of interactions in enhancing the condensate depletion of each component in a mixture as compared to the case when each component is in a *separate trap of its own*. To the best of our knowledge, this has not been done in the previous literature on mixed Bose gases up to this date. We present physics associated with the effect of intraspecies and interspecies interactions on the condensate properties of mixed Bose gases. We find that

(a) The mixing of two Bose gases in a trap enhances the condensate depletion of each gas as compared to the case when either one is in a separate trap of its own. In both cases of attractive and repulsive interactions the reduction in the available volume for condensate formation due to mixing plays a key role in the enhancement of the depletion. In the case of attractive interspecies interaction the enhanced depletion may be further driven by the liquefaction of the Bose gases at the higher densities and the release of energy.

(b) When the condensates are phase separated due to strong repulsive interspecies interactions, the core remains stable and is not "squeezed" substantially by the shell. Complete mixing is still possible up to some repulsion threshold.

(c) According to Refs. [16], our mixtures are stable because they are spherically symmetric.

(d) We anticipate that the healing length of a 1BEC changes upon mixing it with a second component into the system.

(e) In the case of complete phase separation, although the density of the shell is much smaller than the core, substantial depletion is still observed in the shell triggered by the presence of large bosons in the shell.

(f) In the case of intercomponent attraction a 2BEC behaves similarly to a 1BEC as the two components are completely mixed and allow the condensates of either component to migrate towards the edges of the trap at the higher densities. This is contrary to the somewhat opposite case of repulsive interspecies interactions where the condensate of the core is pushed back towards the center of the trap.

(g) Finally, the HC potentials provide a strong stabilizing mechanism for the Bose gases with attractive interactions.

ACKNOWLEDGMENTS

APPENDIX: MEAN-FIELD MODEL FOR THE ESTIMATION OF THE MIXTURE ENERGIES

We consider two mixed Bose gases of N_1 and N_2 particles, HC diameters a_c and b_c, and bosonic masses m_1 and m_2,

respectively, where initially the interspecies interactions are set to zero. That means the two Bose gases are initially independent of each other and both of them are concentric spheres at the trap center. We then construct a rough model that describes the energy of a boson-boson mixture by using the following assumptions. In our estimate for the energies, we derive our concepts from a paper by Ao and Chui [15] who gave a simplified expression for the total energy of an inhomogeneous binary Bose gas,

$$E = \frac{1}{2}\left(G_{11}\frac{N_1^2}{V} + G_{22}\frac{N_2^2}{V} + \sqrt{G_{11}G_{22}}\frac{N_1N_2}{V} \right), \quad \text{(A1)}$$

where $G_{ij}=4\pi\hbar^2 a_{ij}/m_{ij}$ are the interaction parameters, a_{12} is the interspecies and a_{ii} is the intraspecies *s*-wave scattering length, m_{ii} is the mass of a boson in one component, m_{12} is the reduced mass, and *V* is the volume of the gas. This expression neglects the kinetic energy (quantum pressure) of each component. We modify this expression by replacing the first two terms on the right-hand-side by the Thomas-Fermi (TF) energy of each component. We use trap units in terms of component 1, i.e., $a_{ho}=\sqrt{\hbar/m_1\omega_1}$ and $\hbar\omega_1$ for both systems as done before. The TF energy for each component is then

$$E_{TF,i} = \frac{5}{7}N_i\mu_i, \quad \text{(A2)}$$

where $i=1,2$, $\mu_1=\frac{1}{2}(15N_1a_c)^{2/5}$ is the chemical potential of component 1 and

$$\mu_2 = \frac{1}{2}(15N_2b_c)^{2/5}\left(\frac{m_2}{m_1}\right)^{1/5} \quad \text{(A3)}$$

is that of component 2. The TF radius of component 1 is $R_{TF,1}=(15N_1a_c)^{1/5}$ and that of component 2 is

$$R_{TF,2} = (15N_2b_c)^{1/5}\left(\frac{m_1}{m_2}\right)^{2/5}. \quad \text{(A4)}$$

Imagine now switching the interspecies interactions on such that the Bose gas with the larger HC diameter is expelled towards the edges of the trap and forms a shell. The shell would then lie approximately at the TF radius of the core away from the center of the trap. The volume of the cloud is then approximately $V=4\pi R_{TF,1}^3/3$ if $a_c<b_c$ and $4\pi R_{TF,2}^3/3$ if $a_c>b_c$. Thus, the size of the cloud is largely determined by the core in the case of moderate repulsive interactions. In order to calculate its energy, we therefore assume a superposition of its initial TF energy when both mutually noninteracting components are localized at the center of the trap and an approximate potential energy for the particles of the shell formed at the edges of the trap after switching on the interspecies interactions. As a result, component 2 gains additional potential energy beyond $E_{TF,2}$ when it becomes a shell. An estimate for the potential energy of the shell is

$$V_{trap} = \frac{1}{2}N_1 m_1 \omega_{ho}^2 R_{TF,2}^2/\hbar\omega_{ho} = \frac{1}{2}N_1\left(\frac{m_1}{m_2}\right)^{4/5}(15N_2b_c)^{2/5} \quad \text{(A5)}$$

if component 1 forms a shell and

$$V_{trap} = \frac{1}{2} N_2 m_2 \omega_{ho}^2 R_{TF,1}^2 / \hbar \omega_{ho} = \frac{1}{2} N_2 \left(\frac{m_2}{m_1} \right) (15 N_1 a_c)^{2/5} \tag{A6}$$

if component 2 forms a shell. [Note that in (A5) and (A6) we imply $R_{TF,i}/a_{ho} \to R_{TF,i}$.] That is, we used

$$\frac{\sum_{i=1}^{n_1} m_1 r_{1i}^2}{\sum_{i=1}^{n_1} m_1} = \langle r_1^2 \rangle \approx R_{TF,2}^2 \tag{A7}$$

and

$$\frac{\sum_{i=1}^{n_2} m_2 r_{2i}^2}{\sum_{i=1}^{n_2} m_2} = \langle r_2^2 \rangle \approx R_{TF,1}^2 \tag{A8}$$

in estimating the radius of gyration of the core. Note that $\Sigma_{i=1}^{N_k} m_k = N_k m_k$ ($k=1$ or 2) is the total mass of either component as all the particles in a component have the same mass. The interspecies interactions can be calculated according to Eq. (A1) as follows:

$$E_{int} = \sqrt{G_{11} G_{22}} \frac{N_1 N_2}{V}. \tag{A9}$$

Gathering all the previous terms together, the total energy of the mixture is then

$$E^{MFA}(N_1 + N_2) \approx \frac{5}{14} [N_1 (15 N_1 a_c)^{2/5} + N_2 (15 N_2 b_c)^{2/5} (m_2/m_1)^{1/5}] + 3 [a_c b_c (m_1/m_2)]^{1/2} N_1 N_2$$

$$\times \begin{cases} R_{TF,1}^{-3}, & a_c < b_c \\ R_{TF,2}^{-3}, & a_c > b_c \end{cases} + \begin{cases} \frac{1}{2} N_1 (m_1/m_2)^{4/5} (15 N_2 b_c)^{2/5}, & a_c > b_c \\ \frac{1}{2} N_2 (m_2/m_1) (15 N_1 a_c)^{2/5}, & a_c < b_c, \end{cases} \tag{A10}$$

where as a reminder $\omega_1 = \omega_2$.

[1] C. J. Myatt, E. A. Burt, R. W. Ghrist, E. A. Cornell, and C. E. Wieman, Phys. Rev. Lett. **78**, 586 (1997).

[2] B. D. Esry, Chris H. Greene, James P. Burke, and John L. Bohn, Phys. Rev. Lett. **78**, 3594 (1997).

[3] T. L. Ho and C. V. Ciobanu, J. Low Temp. Phys. **135**, 257 (2004).

[4] V. S. Shchesnovich, A. M. Kamchatnov, and R. A. Kraenkel, Phys. Rev. A **69**, 033601 (2004).

[5] K. Kasamatsu and M. Tsubota, J. Low Temp. Phys. **134**, 677 (2004).

[6] T. L. Ho and V. B. Shenoy, Phys. Rev. Lett. **77**, 3276 (1996).

[7] H. Pu and N. P. Bigelow, Phys. Rev. Lett. **80**, 1130 (1998).

[8] D. Schumayer and B. Apagyi, Phys. Rev. A **69**, 043620 (2004).

[9] S. T. Chui, H. Chui, H. L. Shi, W. M. Liu, and W. M. Zheng, Physica B (Amsterdam) **329**, 36 (2003).

[10] H. L. Shi, W. M. Zheng, and S. T. Chui, Phys. Rev. A **61**, 063613 (2000).

[11] R. A. Barankov, Phys. Rev. A **66**, 013612 (2002).

[12] E. A. Cornell, D. S. Hall, M. R. Matthews, and C. E. Wieman, J. Low Temp. Phys. **113**, 151 (1998).

[13] A. Sinatra and Y. Castin, Eur. Phys. J. D **8**, 319 (2000).

[14] D. S. Hall, M. R. Matthews, J. R. Ensher, C. E. Wieman, and E. A. Cornell, Phys. Rev. Lett. **81**, 1539 (1998).

[15] P. Ao and S. T. Chui, Phys. Rev. A **58**, 4836 (1998).

[16] M. Trippenbach, K. Góral, K. Rzazewski, B. Malomed, and Y. B. Band, J. Phys. B **33**, 4017 (2000).

[17] H. Ma and T. Pang, Phys. Lett. A **351**, 92 (2006).

[18] P. G. Kevredekis, H. E. Nistazakis, D. J. Frantzeskakis, B. A. Malomed, and R. Carretero-González, Eur. Phys. J. D **28**, 181 (2004).

[19] Zachary Dutton and Charles W. Clark, Phys. Rev. A **71**, 063618 (2005).

[20] W. J. Mullin, R. Krotkov, and F. Laloë, Phys. Rev. A **74**, 023610 (2006).

[21] M. Nakano, S. Ohta, R. Kishi, H. Takahashi, and S. Furukawa, Eur. Phys. J. D **38**, 523 (2006).

[22] D. C. Roberts and M. Ueda, Phys. Rev. A **73**, 053611 (2006).

[23] M. H. Anderson, J. R. Ensher, M. R. Matthews, C. E. Wieman, and E. A. Cornell, Science **269**, 198 (1995).

[24] C. C. Bradley, C. A. Sackett, J. J. Tollett, and R. G. Hulet, Phys. Rev. Lett. **75**, 1687 (1995).

[25] C. A. Sackett, H. T. C. Stoof, and R. G. Hulet, Phys. Rev. Lett. **80**, 2031 (1998).

[26] J. G. Kim and E. K. Lee, Phys. Rev. E **65**, 066201 (2002).

[27] G. Modugno, M. Modugno, F. Riboli, G. Roati, and M. Inguscio, Phys. Rev. Lett. **89**, 190404 (2002).

[28] G. Modugno, G. Ferrari, G. Roati, R. J. Brecha, A. Simoni, and M. Inguscio, Science **294**, 1320 (2001).

[29] M. Mudrich, S. Kraft, K. Singer, R. Grimm, A. Mosk, and M.

Weidemüller, Phys. Rev. Lett. **88**, 253001 (2002).

[30] P. Maddaloni, M. Modugno, C. Fort, F. Minardi, and M. Inguscio, Phys. Rev. Lett. **85**, 2413 (2000).

[31] M. R. Matthews, B. P. Anderson, P. C. Haljan, D. S. Hall, C. E. Wieman, and E. A. Cornell, Phys. Rev. Lett. **83**, 2498 (1999).

[32] M. R. Matthews, D. S. Hall, D. S. Jin, J. R. Ensher, C. E. Wieman, E. A. Cornell, F. Dalfovo, C. Minniti, and S. Stringari, Phys. Rev. Lett. **81**, 243 (1998).

[33] J. L. DuBois and H. R. Glyde, Phys. Rev. A **63**, 023602 (2001).

[34] A. R. Sakhel, J. L. DuBois, and H. R. Glyde, Phys. Rev. A **66**, 063610 (2002).

[35] G. E. Astrakharchik, D. Blume, S. Giorgini, and B. E. Granger, Phys. Rev. Lett. **92**, 030402 (2004).

[36] N. Metropolis, A. W. Rosenbluth, M. N. Rosenbluth, A. H. Teller, and E. Teller, J. Chem. Phys. **21**, 1087 (1953).

[37] W. H. Press, S. A. Teukolsky, W. T. Vetterling, and B. B. Flannery, *Numerical Recipes in C*, 2nd ed. (Cambridge University Press, New York, 1999).

[38] S. T. Chui and V. N. Ryzhov, Phys. Rev. A **69**, 043607 (2004).

[39] E. G. M. van Kempen, S. J. J. M. F. Kokkelmans, D. J. Heinzen, and B. J. Verhaar, Phys. Rev. Lett. **88**, 093201 (2002).

[40] S. Geltman and A. Bambini, Phys. Rev. Lett. **86**, 3276 (2001).

[41] B. Gao, J. Phys. B **36**, 2111 (2003).

[42] W. J. Mullin (private communications).

[43] S. Giorgini, J. Boronat, and J. Casulleras, Phys. Rev. A **60**, 5129 (1999).